Hindawi
Geofluids
Volume 2022, Article ID 8784398, 12 pages
https://doi.org/10.1155/2022/8784398

Research Article

Development of Similar Materials for Liquid-Solid Coupling and Its Application in Water Outburst and Mud Outburst Model Test of Deep Tunnel

Yanhui Guo,[1,2] **Yi Yang**,[1,2] **Zhijun Kong**,[3] **and Jin He**[3]

[1]*Faculty of Public Safety and Emergency Management, Kunming University of Science and Technology, Kunming 650093, China*
[2]*Key Laboratory of Early Rapid Identification, Prevention and Control of Geological Diseases in Traffic Corridor of High Intensity Earthquake Mountainous Area of Yunnan Province, Kunming 650093, China*
[3]*College of Civil and Architectural Engineering, Yunnan Agricultural University, Kunming 650201, China*

Correspondence should be addressed to Yanhui Guo; guoyanhui0818@kust.edu.cn

Received 1 April 2022; Revised 18 April 2022; Accepted 29 April 2022; Published 21 May 2022

Academic Editor: Hao Wu

In order to explore the evolution mechanism of water and mud inrush, based on the fluid-solid coupling similarity theory and a large number of matching tests, fault similar materials with mountain sand, gravel, and red clay as raw materials and surrounding similar rock materials with mountain sand, red clay, cement, and water as raw materials are developed. Similar materials' physical and mechanical properties and hydraulic properties with different ratios are tested and analyzed. The results show that the red clay content influences the mechanical properties of similar materials and their hydraulic properties, and the gravel substrate mainly influences the fault permeability coefficient. Similar material can be adjusted within a certain range of mechanical parameters. The material is simple and suitable for developing similar materials for different low and medium strength rock masses. Finally, a similar material was used in a model test of the tunnel fault fracture zone to reveal the mechanism of water and mud bursts in the tunnel. The study results can be used as a reference for the development of similar materials for tunnel fracture zone surrounding rocks.

1. Introduction

Due to the rapid growth of economic construction, the need for national security, and the development of national resource areas in the center and west of the country, the development of underground space in China is constantly moving deeper into the earth, with deep resource extraction and various types of transportation, water conservancy, and hydropower engineering construction being the most significant [1, 2]. However, the environment in which the deep tunnel project is located often has high in situ stress, temperature, and groundwater pressure [3, 4]; this reason has led to rock bursts and water and mud bursts during tunnel construction. Mud inrush disasters are the most common and cause serious casualties and economic losses [5, 6]. Studying the occurrence and development of sudden water flow in tunnels has important theoretical significance and engineering application value for preventing and managing disasters [7, 8]. The real engineering environment is often very complex, and it is difficult to carry out a comprehensive analysis and study based on theoretical and numerical calculations alone [9, 10]. The geomechanical model test is a more accurate reproduction of the actual geological conditions on-site. It can effectively analyze and discuss the multifield information on the evolution of sudden water and mud hazards, which effectively studies the evolution of the laws and mechanisms of sudden water and mud hazards [11–13]. The key to successful model tests is developing similar materials for fluid-solid coupling [14, 15]. As the geological conditions vary greatly from region to region and tunnel to tunnel, the choice of aggregates and binders for similar materials varies, making it necessary to develop a new similar material based on the theory of similarity.

Table 1: The main similarity relationship between the prototype and the model of fluid-structure interaction similar materials.

Similar type	Stress	Source and sink	Storage coefficient	Penetration factor
Similar constant	$C_\sigma = C_\gamma C_l = C_E = C_R = C_C$	$C_W = 1/\sqrt{C_l}$	$C_S = 1/\left(C_\gamma \sqrt{C_l}\right)$	$C_K = \sqrt{C_l/C_\gamma}$

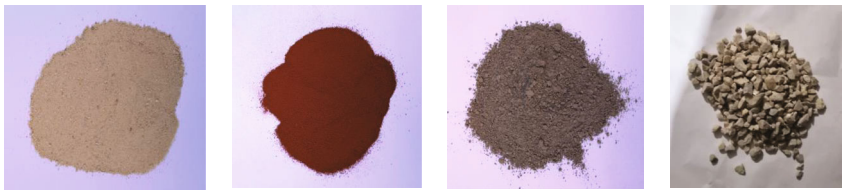

(a) Mountain sand (b) Red clay (c) Cement (d) Gravel

Figure 1: Raw materials for preparing similar materials.

In order to develop similar materials that meet the test requirements, scholars have conducted studies using different raw materials. Zuo et al. [16] studied the similar materials of limestone; analyzed the influence of various or single factors such as aggregate, cement, and curing methods on the strength of similar materials; and pointed out that the rock mass medium can simulate by quartz sand, gypsum, and cement. Huang et al. [17] used cement, gypsum, and sand as raw materials in many proportioning tests to formulate a fluid-solid coupled similar material that met the test requirements. The effect of cement and aggregates on the mechanical and hydraulic properties of the material was analyzed, and the results showed that the ash-sand ratio and paste-sand ratio had a large effect on most of the mechanical and hydraulic properties of the similar material. Zhang and Hou [18] developed a "solid-liquid" two-phase model material using paraffin wax as a cementing agent, solving similar materials' water disintegration. Huang et al. [19] identified the similar materials of clay water barrier as quartz sand, bentonite, silicone oil, and vaseline, which solved the problem of plasticity and hydrology of water barrier simulation. Hu et al. [20] used cement, gravel, gypsum, talcum powder, and calcimine to simulate the rock layer and red mud to simulate the weak water barrier and achieved better results in the large-scale fluid-solid coupling simulation test. Zhang et al. [21] used sand, lime, and gypsum as raw materials to prepare similar materials. They studied the effects of different ratios of raw materials and the number of maintenance days on the materials through proportioning tests. The results showed that the degree of influence of each factor on similar materials was in the order of sand to glue ratio, grey to paste ratio, and maintenance days. Li et al. [22] used paraffin cement to create similar water-repellent materials and analyzed the effects of various proportions of materials and maintenance temperatures on the performance of the specimens. Han et al. [23] used medium-coarse sand, permeable concrete reinforcement, and cement to develop a pore rock body and successfully applied it to model tests. The results indicated that the similar material had stable mechanical properties and was suitable for conducting large-scale physical simulation tests of coupled failure damage modes of the structure and the surrounding rock body. Li et al. [24–26] proposed a unique material, SCVO, which was successfully used in a water surge experiment in a subsea tunnel to reveal the changes in cavern wall pressure and movement of the walls and seepage during the construction of the sub-sea tunnel.

Although much research on fluid-solid coupled similar materials has made rapid progress, the current development of similar materials is mostly conducted for specific projects through many ratio tests to determine the most suitable ratio. The previous similar materials are mostly focused on solving the easy disintegration of materials in water; its similarity simulation degree is poor, ignoring the control of the solid mechanical properties of materials and water rationality. Therefore, it is necessary to further research on fluid-solid coupled similar materials. Therefore, there is a need for further research on fluid-solid coupled with similar materials. In this paper, based on the similarity theory and through a large number of proportional tests, a similar material with simple components, low price, easy fabrication, and suitable for most of the rock masses was developed and successfully applied in the model test of water and mud protrusion in the tunnel fracture zone.

2. Similarity Theory and Physical Model Test Similarity Ratio

2.1. Fluid-Solid Coupling Similarity Theory. Similar model tests need to satisfy geometric similarity, the kinetic similarity among models and archetypes, and the physical similarity among materials or media [27–29]. In studying the possible mechanical phenomena of the prototype, rock pressure distribution, and other geotechnical problems, due to the objective conditions, it is often necessary to indirectly solve the problem through the similarly transformed model.

To make the model test closer to the actual situation in the field, Hu et al. [30], based on the understanding of the

(a) Weigh the material (b) Stir well (c) Pouring test piece

(d) Stratification (e) Pouring completed (f) Demoulding

Figure 2: Pouring process of similar material specimen.

Table 2: Quality proportion of similar materials in different proportions.

Material ratio	Quality as a percentage (%)			
	Mountain sand	Red clay	Cement	Water
12 : 0.15 : 0.7 : 1.3	84.81	1.06	4.94	9.19
12 : 0.35 : 0.7 : 1.3	83.62	2.44	4.88	9.06
12 : 0.55 : 0.7 : 1.3	82.47	3.78	4.81	8.94
12 : 0.75 : 0.7 : 1.3	81.36	5.08	4.75	8.81
12 : 0.95 : 0.7 : 1.3	80.27	6.35	4.68	8.70
12 : 1.15 : 0.7 : 1.3	79.21	7.59	4.62	8.58
12 : 1.35 : 0.7 : 1.3	78.18	8.79	4.56	8.47
12 : 1.55 : 0.7 : 1.3	77.17	9.97	4.50	8.36

fluid-consolidation total, deduced that the solid-fluid-solid-fluid is reasonable by using a continuous intermediate combined mathematical model, as shown in the following formula:

$$C_G \frac{C_u}{C_l^2} = C_\lambda \frac{C_e}{C_l} = C_G \frac{C_e}{C_l} = C_\gamma = C_\rho \frac{C_u}{C_t^2}, \quad (1)$$

where C is the similarity scale, G is the shear modulus of elasticity, u is the displacement, l is the model size, λ is the Lamé constant, e is the volume strain, γ is the bulk weight, ρ is the density, and t is time.

It can be deduced from formula (1) that the model is similar $C_G = C_\lambda$; the geometry is similar $C_u = C_e C_l$, because the geometry still needs to be similar after deformation, it can only $C_e = 1$, then $C_u = C_l$; the gravity is similar $C_G C_e = C_\gamma C_l$, the conversion relationship between the shear elastic modulus and the elastic modulus is $G = E/(2(1+\mu))$, we can see $C_G = C_e$, then, $C_e = C_\gamma C_l$; stress similarity $C_\sigma = C_E C_e$, while $C_e = 1$, then, $C_\sigma = C_\gamma C_l$; time similarity $C_G C_u / C_l^2 = C_\rho C_u / C_l^2$, $C_\gamma = C_\rho C_u / C_t^2$, and $C_\gamma = C_\rho C_g$, can be obtained $C_t = \sqrt{C_l}$.

Since the similar material is homogeneous material, the respective penetration coefficients are the same, that is, $K_x = K_y = K_z = K$, according to the existing similar relationship, the prototype material is obtained:

$$\frac{C_K C_P}{C_x^2} = \frac{C_K C_P}{C_y^2} = \frac{C_K C_P}{C_z^2} = \frac{C_S C_P}{C_t} = \frac{C_e}{C_t} = C_w. \quad (2)$$

In the formula, P is the water pressure, and w is a source sink item.

Based on the above analysis, the main similar relationship between the flow-solid coupling similar material model and the prototype is shown in Table 1.

3. Development of Similar Materials for Fluid-Solid Coupling

3.1. Selection of Similar Materials and Raw Materials. The development of similar materials requires, on the one hand, to meet the progressive nature of the failure process in the liquid state. On the other hand, they must not soften easily when in contact with water. At the same time, it is important to ensure that the material's mechanical properties are close to those of the original. According to the current research results, following the principles of easy access to materials, low cost, and simple production, mountain sand, red clay unique to the Yunnan-Guizhou plateau, slag silicate cement, and water were selected as raw materials for similar materials in the surrounding rock, gravel as the raw material of fault-like material. The basic composition of similar materials is shown in Figure 1. In preparing similar materials, mountain sand is used as aggregate, C32.5 slag silicate cement as cementing material, water as auxiliary material, and red clay as a conditioning agent. The red clay used for

(a) Compressive strength test (b) Testing machine control software

Figure 3: Uniaxial compressive strength test of similar materials.

Table 3: Test values of bulk density and uniaxial compressive strength of similar materials.

Proportion of red clay	Specimen number	Bulk density γ (kN/m^3)	Mean bulk weight $\bar{\gamma}$ (kN/m^3)	Compressive strength σ (MPa)	Average compressive strength (MPa)
	1-1	18.34		0.34	
1.06	1-2	18.17	18.09	0.39	0.37
	1-3	17.76		0.37	
	2-1	18.61		0.47	
2.44	2-2	18.75	18.73	0.54	0.51
	2-3	18.82		0.52	
	3-1	18.37		0.44	
3.78	3-2	18.33	18.31	0.51	0.47
	3-3	18.24		0.46	
	4-1	18.54		0.42	
5.08	4-2	18.26	18.44	0.39	0.42
	4-3	18.53		0.45	
	5-1	18.10		0.40	
6.35	5-2	18.27	18.16	0.44	0.40
	5-3	18.11		0.37	
	6-1	18.26		0.58	
7.59	6-2	18.65	18.39	0.62	0.61
	6-3	18.26		0.64	
	7-1	18.38		0.51	
8.79	7-2	18.06	18.24	0.48	0.50
	7-3	18.27		0.52	
	8-1	17.76		0.55	
9.97	8-2	17.69	17.77	0.61	0.55
	8-3	17.86		0.48	

the fault has a particle size of less than 1 mm, and the gravel has a subgrain range of 4.75 mm to 9.5 mm.

3.2. Pouring Test Pieces of Similar Materials to the Model. First, weigh the corresponding raw materials according to the designed proportioning plan, then mix the mountain sand, red clay, and cement in a mixer. After thoroughly mixing, add the preweighed water and continue mixing until the mixture is uniform, and finally, the mixture is entirely similar. The material is shoveled into a prefabricated PVC pipe with a diameter of 50 mm and a height of 100 mm with a small spatula and tamped in three layers. After the similar material is poured, it is cured at room temperature for three days. After the curing is completed, the mold is removed with a hacksaw. The pouring process of the test piece is as follows, as shown in Figure 2.

As the particle size of red clay is smaller than that of mountain sand and has a specific viscosity, when preparing similar materials, by controlling the approximate ratio of mountain sand, cement, and water, and then appropriately increasing the content of red clay, the purpose of adjusting the permeability of the material can be achieved. Referring to many studies both nationally and internationally, after a large number of ratio attempts, when proportioning similar

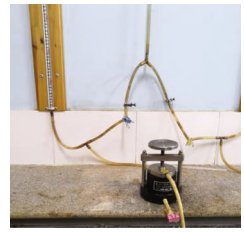

(a) Glass tube water injection

(b) Exhaust bottom air

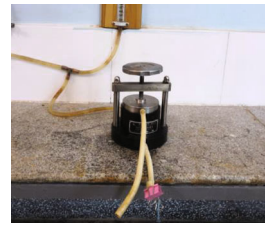

(c) Clamping hose starts to seep

Figure 4: Permeation test operation procedure.

Table 4: Permeability coefficient of surrounding rock and fault similar materials.

Mixing ratio of surrounding rock materials			Fault material ratio		
Mountain sand : red clay : cement : water	Proportion of red clay (%)	Permeability coefficient (cm/s)	Red clay : mountain sand : gravel	Percentage of gravel (%)	Permeability coefficient (cm/s)
12 : 0.15 : 0.7 : 1.3	1.06	0.000142	1 : 1 : 0.4	16.67	0.000539
12 : 0.35 : 0.7 : 1.3	2.44	0.00013	1 : 1 : 0.5	20.00	0.000675
12 : 0.55 : 0.7 : 1.3	3.78	0.000118	1 : 1 : 0.6	23.08	0.000771
12 : 0.75 : 0.7 : 1.3	5.08	0.0000803	1 : 1 : 0.7	25.92	0.000857
12 : 0.95 : 0.7 : 1.3	6.35	0.0000554	1 : 1 : 0.8	28.57	0.000892
12 : 1.15 : 0.7 : 1.3	7.59	0.0000429	1 : 1 : 0.9	31.04	0.000982
12 : 1.35 : 0.7 : 1.3	8.79	0.0000904			
12 : 1.55 : 0.7 : 1.3	9.97	0.0000655			

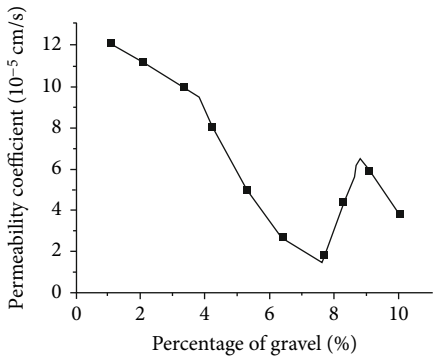

(a) Similar materials in the surrounding rock

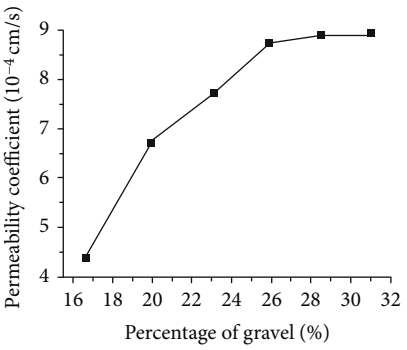

(b) Fault similar material

Figure 5: Test values of permeability coefficients of similar materials with different ratios.

materials, control the percentage of sand, cement, and water for each group to be 12 : 0.7 : 1.3. The proportion of red clay in the initial proportioning scheme was 0.15, and the proportion of red clay in the subsequent schemes was increased by 0.2 compared with the previous proportion. A total of 8 proportions were designed throughout the experiment. The specific values of each proportioning scheme are shown in Table 2.

Table 5: Water absorption and softening coefficient of similar materials after immersion in water.

Proportion of red clay	Specimen number	Water absorption (%)	Average water absorption (%)	Strength after immersion (MPa)	Mean intensity (MPa)	Softening factor
	1-4	4.31		0.36		
1.06	1-5	5.16	4.77	0.32	0.35	0.95
	1-6	4.83		0.37		
	2-4	4.55		0.45		
2.44	2-5	4.46	4.43	0.48	0.47	0.92
	2-6	4.28		0.47		
	3-4	3.49		0.45		
3.78	3-5	3.43	3.67	0.38	0.42	0.89
	3-6	4.08		0.42		
	4-4	2.93		0.35		
5.08	4-5	2.64	2.82	0.33	0.36	0.86
	4-6	2.89		0.41		
	5-4	2.94		0.31		
6.35	5-5	3.56	3.51	0.34	0.34	0.85
	5-6	4.04		0.37		
	6-4	6.11		0.52		
7.59	6-5	5.63	5.77	0.49	0.48	0.79
	6-6	5.56		0.44		
	7-4	3.35		0.36		
8.79	7-5	3.87	3.56	0.42	0.39	0.78
	7-6	3.47		0.38		
	8-4	3.53		0.43		
9.97	8-5	3.86	3.86	0.41	0.41	0.75
	8-6	4.19		0.39		

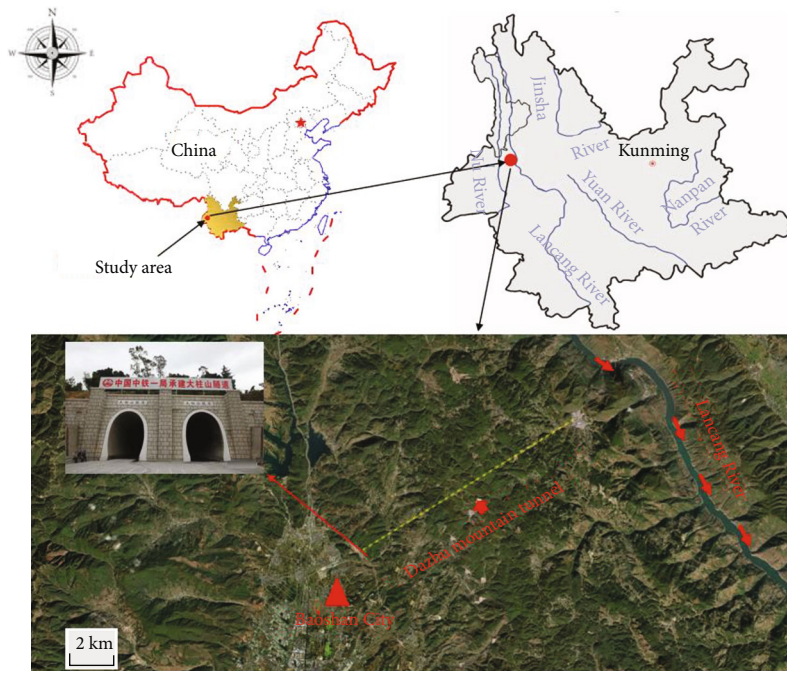

Figure 6: Location plan of Dazhu Mountain Tunnel.

Figure 7: Model test system.

3.3. Physical and Mechanical Properties Test of Similar Materials. Before starting the test, it is necessary to carefully grind both ends of the specimen with sandpaper so that the nonparallelism error of the two ends is less than 0.05 mm, and the quality and height of the specimen after grinding are strictly controlled. The density and bulk density of each specimen can be calculated according to the cross-sectional area of the specimen. Similar materials' uniaxial compressive strength parameters were carried out using the electronic universal testing machine developed by Shenzhen Xinsansi Material Testing Co., Ltd., as shown in Figure 3.

In order to eliminate test errors, the uniaxial compressive strength test is carried out by selecting three specimens of the same proportion for testing. The test results are taken as the mean of the three specimens. Table 3 shows the test results of the test pieces' bulk density and uniaxial compressive strength under different proportioning schemes. According to the results, the bulk weight of similar materials ranged from 17.77 kN/m^3 to 18.73 kN/m^3, and the uniaxial compressive strength ranged from 0.37 MPa to 0.61 MPa under different raw material proportions. Similar materials can be adjusted in a wide range of capacity and compressive strength so that when formulating similar materials, suitable raw material ratios can be selected according to the model surrounding rock parameters obtained through the conversion of similar theoretical formulas.

3.4. Similar Material Hydraulic Performance Test

3.4.1. Permeability Coefficient Test. As the permeability coefficients of similar materials were very small in model tests, the volume of water permeated was very small. The errors of the coefficients of permeability of materials measured by the constant head test method were large, so the tests were carried out using the variable head test method to measure the head of the surrounding rock with different ratios. The permeability test procedure is shown in Figure 4.

At the end of the permeation test, the permeation coefficients of similar materials were calculated using equation (3) to obtain the permeation coefficients of similar materials for different proportioning conditions.

$$k = 2.3\frac{aL}{A(t_2 - t_1)}\lg\frac{H_1}{H_2}, \tag{3}$$

where k is the permeability coefficient; a is the cross-sectional area of the variable head tube; L is the height of the specimen; A is the cross-sectional area of the specimen; t_1 and t_2 are the reading start time and termination time; H_1 and H_2 are the starting head and termination head.

Table 4 shows the test results of permeability coefficients of similar materials of surrounding rock with different ratios and similar materials of faults. Figure 5 shows the test values of permeability coefficients of similar materials with different proportions.

As shown in Figure 5, the permeability coefficients of similar materials show a fluctuating process of decreasing, then increasing, and then decreasing as the red clay content increases. When the proportion of red clay increased from 1.06% to 7.59%, the permeability coefficient of the faulted similar material specimens gradually decreased from 1.42×10^{-4} cm/s to 4.29×10^{-5} cm/s. In comparison, when the proportion of red clay increased to 8.79% and 9.97%, the permeability coefficients of the materials became 9.04×10^{-5} cm/s and 6.55×10^{-5} cm/s, respectively. In the development of similar materials, the material's permeability can be reduced by increasing the content of red clay appropriately.

It can also be seen that the material permeability coefficient shows a gradual increase as the percentage of gravel substrate in the fault-like material increases. When the percentage of gravel substrate increases from 16.67% to 31.04%, the permeability coefficient of fault similar material increases from 5.39×10^{-4} cm/s to 9.82×10^{-4} cm/s. The change in permeability coefficient of fault material may be due to the increase of coarse particles in the material, which leads to the inability of fine particles to be adequately compacted, causing the increase in permeability coefficient.

3.4.2. Physical and Mechanical Properties of Material Saturated with Water. First, similar materials of different proportions were weighed and then immersed in water for 5 hours. At the end of the test, the specimens were removed and left for 20 minutes to weigh the mass of the specimens, followed by precompression strength tests in the uniaxial direction. Table 5 shows the water absorption and softening coefficients of the materials for different red clay content conditions.

From Table 4, it is clear that the water absorption of similar materials in the fault ranges from 2.82% to 5.77%, the uniaxial compressive strength of the material following immersion ranges from 0.34 MPa to 0.48 MPa, and the softening coefficient is between 0.75 and 0.95. Compared with similar materials that have not been immersed in water, the compressive strength of similar materials after immersion has attenuated to varying degrees. As the content of red clay in the material increases, the softening coefficient shows a certain regularity, showing a gradually increasing trend.

4. Application of Water and Mud Outburst Model Test in Tunnel Fault Fracture Zone

4.1. Project Summary. Dazhu Mountain Tunnel is located in the Baoshan section of the Da Rui Railway, between Lancangjiang Station and Baoshan North Station. The whole tunnel is 14,484 m long, with "two horizontal and one flat,"

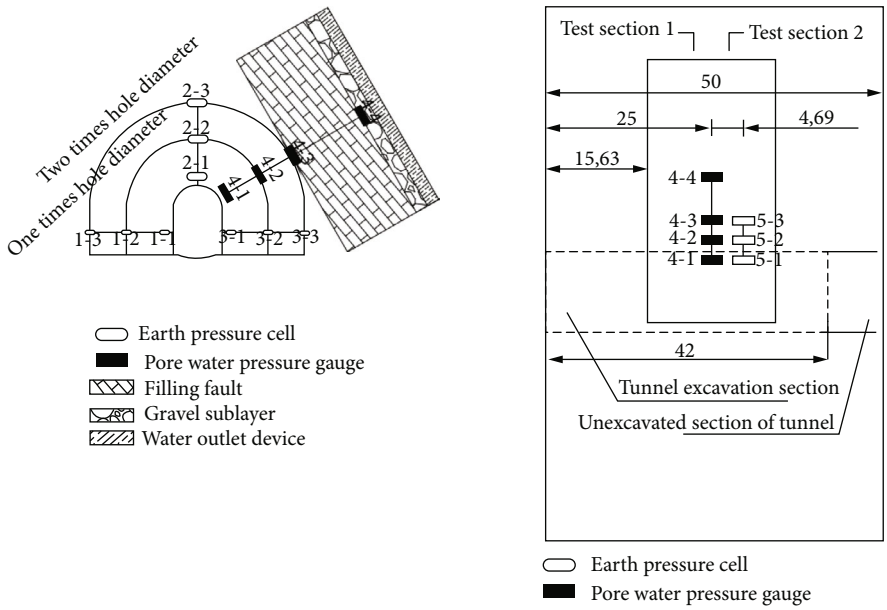

(a) Layout drawing of measuring points on no. 1 monitoring section (b) Monitoring section layout plan

Figure 8: Design of monitoring scheme.

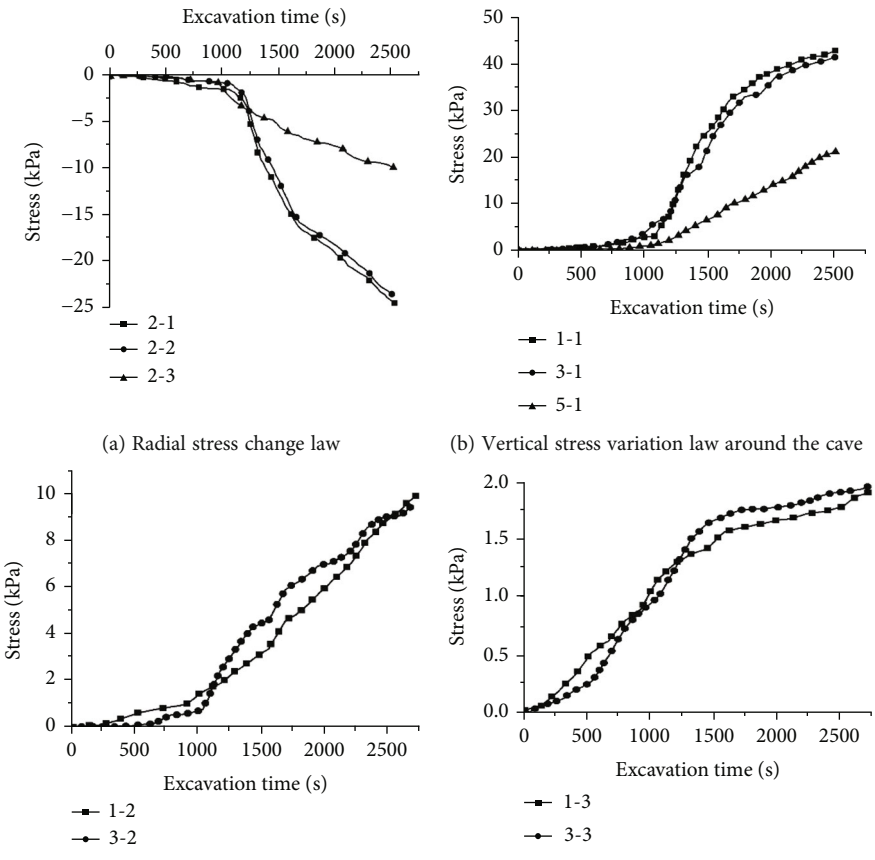

(a) Radial stress change law (b) Vertical stress variation law around the cave

(c) Vertical stress at 1 times the hole diameter (d) Vertical stress at double hole diameter

Figure 9: The law of stress change at the measuring point in the excavation stage.

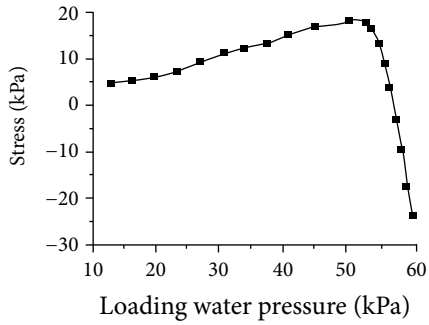

Figure 10: Stress change characteristics of monitoring points in the hydraulic loading stage.

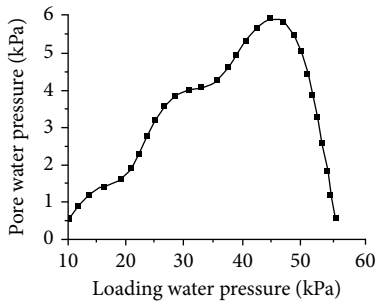

Figure 11: Characteristics of pore water pressure changes at monitoring points during hydraulic loading stage.

of which the tunnel is 13,803 m long in the main tunnel; 680 m in the large span section area, the maximum distance from the top of the tunnel excavation surface to the natural ground is 995 m. The tunnel's slope is a small "herringbone" slope, with a small slope in the exit section and a large slope of 23.5‰ in the other sections. The geological structure of the Dazhu Mountain Tunnel is shown in Figure 6.

4.2. Proportioning Selection of Similar Materials in Model Test. According to the geological survey results, about 30% of the surrounding rocks in the main tunnel cavern are class IV weak surrounding rocks. Therefore, when formulating similar materials, reference is made to the class IV weak surrounding rocks, whose main parameters are capacity 20-23 kN/m^3, compressive strength 38 MPa, and permeability coefficient 4.23×10^{-4} cm/s. The geometric dimensions of the tunnel excavation section are a width of 6.16 m height of 9.41 m. Based on the similarity theory, the capacity of the surrounding rock in ideal conditions is 16.67~19.17 kN/m^3, the compressive strength is 0.396 MPa, and the permeability coefficient is 5.68×10^{-5} cm/s. Testing and analyzing the physical and mechanical properties and hydraulic characteristics of 8 sets of specimens, the ratio of similar materials in the surrounding rock is finally determined as 12 : 0.95 : 0.7 : 1.3. The ratio of red clay content is 6.35%, the capacity of the similar material as 18.16 kN/m^3, the compressive strength is 0.4 MPa, and the permeability coefficient is 5.54×10^{-5} cm/s. The percentage of the components of the fault-like materials is 1 : 1 : 0.4. Under this ratio, the fault permeability coefficient is the smallest and closest to the actual situation.

4.3. Test Summary. Using the Dazhu Mountain tunnel as the research background, a three-dimensional model test of the tunnel's sudden water and mud burst was carried out using a homemade test system [7]. The test system is shown in Figure 7. The model size was 1.0 m × 0.5 m × 1.0 m, with a similar geometry ratio of 80. Based on the actual dimensions of the tunnel, the test excavation section was 7.7 cm wide and 11.76 cm high. The model test section was 12.5 cm thick and 18.75 cm long, two times the excavation diameter, at an angle of 60° to the horizontal, with a stable water outlet device above the section. The test section is buried 500 m deep; the test is similar to the material fill height of about 92 cm, 40 cm above the top of the excavation vault. To compensate for the lack of fill material ground stress, the vertical needs to apply additional graded pressure of about 106 kPa.

After the ground stress reaches the test requirements and the material deformation is stable, the outline of the tunnel is drawn at the excavation site, and the tunnel is excavated and formed along the outline at one time. The excavation length of the tunnel is 42 cm. After the excavation is completed, water is supplied to the fault with an initial water pressure of 10 kPa. After the monitoring data is stabilized under the condition of each water pressure, 5 kPa is loaded to the lower water pressure. When the water inrush in the tunnel occurs, then stop pressurizing. The layout of the monitoring points is shown in Figure 8, in which Figure 8(a) is the layout of the monitoring points on the no. 1 monitoring section, and Figure 8(b) is the side view of the monitoring sections 1 and 2.

4.4. Test Results and Analysis

4.4.1. Surrounding Rock Stress Analysis. As shown in Figure 9(a), radial stress changes at the top of the arch are almost identical during the tunnel excavation, with relatively smooth stresses at the arch measurement points at the beginning of the excavation. The radial stresses at the measured points at the top of the vault decrease sharply after 17 min of excavation, stabilizing after 27 min when the stress trend slows down. It can be seen that the surrounding rock of the tunnel vault is greatly affected by the excavation disturbance. During the excavation process, the radial stress of the surrounding rock near the tunnel face is released sharply, causing the vault stress to drop sharply. After a while, the stress release gradually stabilizes. Stress values remain stable. The stress at monitoring points 2-1 decreased by approximately 24.26 kPa, monitoring points 2-2 by approximately 23.40 kPa, and monitoring point 2-3 by approximately 9.86 kPa during the whole excavation process, indicating that the closer the measuring points to the excavation profile line, the more the excavation affected them.

From Figures 9(b)–9(d), it can be seen that the vertical stresses in the sidewalls on both sides of the tunnel vary very little at the beginning of the excavation and that the vertical stresses in the sidewalls increase abruptly until about 20 min

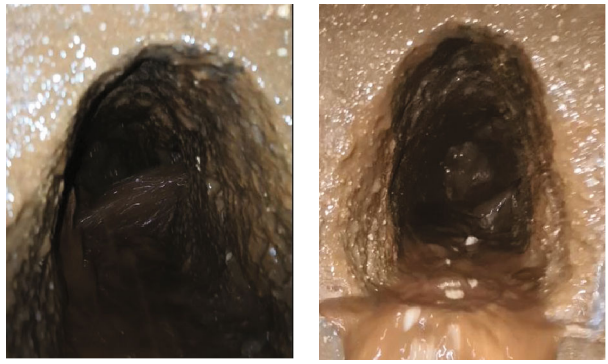

(a) Water burst formation (b) Silt, gravel gushing out

Figure 12: Photograph of water and mud inrush in the tunnel fault fracture zone during the test.

into the excavation, and finally stabilize. The increase in the vertical stresses in the walls on both sides of the perimeter of the tunnel at monitoring section 1 was about 42 kPa, which is twice as high as that in the arch circle at monitoring section 2 (monitoring point 5-1), and the increase in the vertical stresses at monitoring point 3-2 at monitoring section 1 was about 9.49 kPa, and at monitoring point 3-3 was about 1.93 kPa, a difference of 7.56 kPa. The degree of influence is related to the distance from the excavation profile.

4.4.2. Analysis of Surrounding Rock Stress and Pore Water Pressure during Hydraulic Loading Stage. Two times the diameter of the cave, measuring points 3-3, and the perimeter of the cave, measuring points 4-1, were selected to analyze the influence of water pressure on the stress in the surrounding rock and the pore water pressure. Figures 10 and 11 show the characteristic curves of stress and pore water pressure change at the monitoring points during the hydraulic loading stage.

From Figures 10 and 11, it can be seen that during the test, as the loaded water pressure increases, the stress and pore water pressure of the surrounding rock both show a change law of first increasing and then decreasing. When the loaded water pressure increased from 10 kPa to 45 kPa, the internal stress of the model body increased from 3.72 kPa to 16.90 kPa, and the pore water pressure increased from 0.59 kPa to 5.93 kPa, an increase of 905.08%; when the loaded water pressure exceeded 45 kPa, the stress of the surrounding rock and the pore water pressure pile division began to decrease sharply.

The analysis shows that in the rising stage of the pore water pressure at the monitoring point, the water pressure is loaded every three stages. The increase of the pore water pressure gradually slows down. The permeability of the surrounding rock material increases, reducing the rise in pore water pressure. During the stress rise stage of the surrounding rock, the water pressure increases three times. It then decreases, which may be due to the stress concentration at the measurement point during the water pressure loading process. When the water pressure is loaded to 50kPa, the internal stress and pore water pressure grow negatively, the fracture between the fault and the tunnel penetrates, the mud and sand mixture in the fault fill flows out, the water pressure continues to increase, the tunnel is destabilized, and the phenomenon of water and mud emergence occurs. Tunnel fault fragmentation zone is sudden water and mud resulting from excavation disturbance and groundwater seepage. The photos of water and mud inrush in the fractured zone of the tunnel fault during the test are shown in Figure 12.

5. Conclusions

(1) Based on existing methods for the development of similar materials and through extensive proportioning tests, similar material has been developed for most rock masses other than high strength rock masses, with a fault composition of red clay, mountain sand, and gravel, and a perimeter rock composition of mountain sand, red clay, cement, and water

(2) The similar material is influenced by the red clay content, and the gravels mainly influence the fault permeability coefficient. The bulk weight of the material is 17.77 kN/m^3~18.73 kN/m^3. The uniaxial compressive strength is 0.37 MPa~0.61 MPa; the water absorption of the fault material is 2.82% ~5.77%, the uniaxial compressive strength after water immersion is 0.34 MPa~0.48 MPa, and the softening coefficient is 0.75~0.95

(3) Model tests using similar materials have revealed the evolution of sudden water and mud in deeply buried tunnels. The results indicate that the combined effect of tunnel excavation disturbance and groundwater seepage is the main cause of sudden water and mud

Data Availability

The data used to support the findings of this study are included within the article.

Conflicts of Interest

The authors declare that all participants have agreed to the article and no conflict of interest.

Acknowledgments

This study was supported and funded by the Scientific research fund project of Yunnan Provincial Department of Education, China (no. 2022J0065), Key projects of analysis and testing fund of Kunming University of Technology, China (no. 2021T20200145), China Postdoctoral Science Foundation Project (no. 2017M620433), and General projects of Yunnan basic research program (no. 2018FB075).

References

[1] K. Elbaz, S. L. Shen, Y. Tan, and W. C. Cheng, "Investigation into performance of deep excavation in sand covered karst: a case report," *Soils and Foundations*, vol. 58, no. 4, pp. 1042–1058, 2018.

[2] Z. Dou, S. Tang, X. Zhang et al., "Influence of shear displacement on fluid flow and solute transport in a 3D rough fracture," *Lithosphere*, vol. 2021, no. Special 4, 2021.

[3] H. M. Lyu, S. L. Shen, A. N. Zhou, and K. L. Chen, "Calculation of pressure on the shallow-buried twin-tunnel in layered strata," *Tunnelling and Underground Space Technology*, vol. 103, pp. 103465–103465, 2020.

[4] C. Zhu, M. Karakus, M. He et al., "Volumetric deformation and damage evolution of Tibet interbedded skarn under multistage constant-amplitude-cyclic loading," *International Journal of Rock Mechanics and Mining Sciences*, vol. 152, p. 105066, 2022.

[5] N. Zhang, A. N. Zhou, Y. T. Pan, and S. L. Shen, "Measurement and prediction of tunnelling-induced ground settlement in karst region by using expanding deep learning method," *Measurement*, vol. 183, pp. 109700–109700, 2021.

[6] M. S. Abdollahi, M. Najafi, A. Y. Bafghi, and M. F. Marji, "A 3D numerical model to determine suitable reinforcement strategies for passing TBM through a fault zone, a case study: Safaroud water transmission tunnel, Iran," *Tunnelling and Underground Space Technology*, vol. 88, pp. 186–199, 2019.

[7] Y. H. Guo, Z. J. Kong, J. He, and M. Yan, "Development and application of the 3D model test system for water and mud inrush of water-rich fault fracture zone in deep tunnels," *Mathematical Problems in Engineering*, vol. 2021, Article ID 8549094, 16 pages, 2021.

[8] N. Nikadat, M. F. Marji, R. Rahmannejad, and A. Y. Bafghi, "RETRACTED: effect of joint spacing and joint dip on the stress distribution around tunnels using different numerical methods," *Journal of African Earth Sciences*, vol. 123, pp. 193–209, 2016.

[9] B. Fatahi and S. H. R. Tabatabaiefar, "Fully nonlinear versus equivalent linear computation method for seismic analysis of midrise buildings on soft soils," *International Journal of Geomechanics*, vol. 14, no. 4, p. 04014016, 2014.

[10] Y. S. Kim and J. M. Roesset, "Effect of nonlinear soil behavior on inelastic seismic response of a structure," *International Journal of Geomechanics*, vol. 4, no. 2, pp. 104–114, 2004.

[11] P. Castaldo, F. Jalayer, and B. Palazzo, "Probabilistic assessment of groundwater leakage in diaphragm wall joints for deep excavations," *Tunnelling and Underground Space Technology*, vol. 71, pp. 531–543, 2018.

[12] A. B. Bucci, S. B. Prevot, S. Buoso et al., "Impacts of borehole heat exchangers (BHEs) on groundwater quality: the role of heat-carrier fluid and borehole grouting," *Environmental Earth Sciences*, vol. 77, no. 5, pp. 175–183, 2018.

[13] J. Moon and G. Fernandez, "Effect of excavation-induced groundwater level drawdown on tunnel inflow in a jointed rock mass," *Engineering Geology*, vol. 110, no. 3-4, pp. 33–42, 2010.

[14] Z. F. Chu, B. G. Liu, J. L. Sun, J. Shen, Y. Song, and T. Li, "Research on rheological similar material of soft rock based on Burgers model," *Journal of Rock Mechanics and Engineering*, vol. 37, no. 5, pp. 1185–1198, 2018.

[15] W. B. Sun, S. C. Zhang, Y. Y. Li, and C. Lu, "Development application of solid-fluid coupling similar material for floor strata and simulation test of water-inrush deep mining," *Journal of Rock Mechanics and Engineering*, vol. 34, no. S1, pp. 2665–2670, 2011.

[16] B. C. Zuo, C. X. Chen, C. H. Liu, Q. Shen, G. F. Xiao, and X. W. Liu, "Research on similar material experiment," *Rock and Soil Mechanics*, vol. 25, no. 11, pp. 1805–1808, 2004.

[17] Z. Huang, X. Z. Li, S. J. Li, K. Zhao, H. W. Xu, and R. Wu, "Research and development of similar material for liquid-solid coupling and its application in tunnel water-inrush model test," *Journal of Central South University*, vol. 49, no. 12, pp. 3029–3039, 2018.

[18] J. Zhang and Z. J. Hou, "Experimental study on simulation materials for solid-liquid coupling," *Chinese Journal of Rock Mechanics and Engineering*, vol. 23, no. 18, pp. 3157–3161, 2004.

[19] Q. X. Huang, W. Z. Zhang, and Z. C. Hou, "Study of simulation materials of aquifuge for solid-liquid coupling," *Chinese Journal of Rock Mechanics and Engineering*, vol. 29, Supplement 1, pp. 2813–2818, 2010.

[20] Y. Q. Hu, Y. S. Zhao, and D. Yang, "Simulation theory & method of 3D solid-liquid coupling," *Journal of Liaoning Technical University*, vol. 26, no. 2, pp. 204–206, 2007.

[21] X. Y. Zhang, L. Luo, L. F. Xu, and M. Zhao, "Research on quantitative determination method of similar materials ratio," *Coal Mine Safety*, vol. 50, no. 10, 2019.

[22] S. Z. Li, X. D. Feng, S. C. Li, L. P. Li, and G. Y. Li, "Research and development of a new similar material for solid-fluid coupling and its application," *Chinese Journal of Rock Mechanics and Engineering*, vol. 29, no. 2, pp. 281–288, 2010.

[23] T. Han, W. H. Yang, Z. J. Yang, Z. B. Du, Y. Wang, and S. S. Xue, "Development of similar material for porous medium solid-liquid coupling," *Rock and Soil Mechanics*, vol. 32, no. 5, pp. 1411–1417, 2011.

[24] K. Wang, S. C. Li, Q. S. Zhang et al., "Development and application of new similar materials of surrounding rock for a fluid-solid coupling model test," *Rock and Soil Mechanics*, vol. 37, no. 9, pp. y2521–y2533, 2016.

[25] Y. Zhou, S. C. Li, L. P. Li et al., "New technology for fluid-solid coupling tests of underground engineering and its application in experimental simulation of water inrush in filled-type karst conduit," *Chinese Journal of Geotechnical and Engineering*, vol. 37, no. 10, pp. 1232–1240, 2015.

[26] S. C. Li, S. G. Song, L. P. Li et al., "Development on subsea tunnel model test system for solid-fluid coupling and its application," *Journal of Rock Mechanics and Engineering*, vol. 32, no. 5, pp. 883–890, 2013.

[27] Ø. T. Haug, M. Rosenau, K. Leever, and O. Oncken, "On the energy budgets of fragmenting rockfalls and rockslides: insights from experiments," *Journal of Geophysical Research: Earth Surface*, vol. 121, no. 7, pp. 1310–1327, 2016.

[28] F. V. D. Blasio and G. B. Crosta, "Fragmentation and boosting of rock falls and rock avalanches," *Geophysical Research Letters*, vol. 42, no. 20, pp. 8463–8470, 2016.

[29] B. T. Wu, H. H. Zhu, Q. W. Xu, and J. Ming, "Experimental study of similar material for weak surrounding rock mass of class IV," *Rock and Soil Mechanics*, vol. 34, no. 8, pp. 109–116, 2013.

[30] Y. Q. Hu, Y. S. Zhao, and D. Yang, "3D solid-liquid couping experiment study of deformation destruction of coal stope," *Journal of Liaoning Technical University*, vol. 26, no. 2, pp. 204–206, 2007.